Inorganic Chemistry

pubs.acs.org/IC

Article

Organic−Inorganic Two-Dimensional Hybrid Networks Constructed from Pyridine-4-Carboxylate-Decorated Organotin−Lanthanide Heterometallic Antimotungstates

Huifen Hu, Jingjing Pang, Peijun Gong, Lijuan Chen,* and Junwei Zhao*

Cite This: *Inorg. Chem.* 2020, 59, 11287−11297

Read Online

ACCESS | Metrics & More | Article Recommendations | Supporting Information

ABSTRACT: Six organic−inorganic hybrid pyridine-4-carboxylate-decorated organotin (OT)−lanthanide (Ln) heterometallic antimotungstates $[Ln(H_2O)_6(pca)]H[Sn(CH_3)_2(H_2O)]_3[B\text{-}\beta\text{-}SbW_9O_{33}]\cdot 12H_2O$ [Ln = La^{3+} (**1**), Ce^{3+} (**2**), Pr^{3+} (**3**), Nd^{3+} (**4**), Sm^{3+} (**5**), Eu^{3+} (**6**); Hpca = isonicotinic acid] have been prepared with the help of the structure-directing effect of the trivacant $[B\text{-}\alpha\text{-}SbW_9O_{33}]^{9-}$ segment toward $[(CH_3)_2Sn]^{2+}$ and Ln^{3+} ions in an acidic water medium. The prominent architecture characteristic is that their structural units consist of a trivacant $[B\text{-}\beta\text{-}SbW_9O_{33}]^{9-}$ segment stabilized by three $[Sn(CH_3)_2(H_2O)]^{2+}$ groups and a $[Ln(H_2O)_6(pca)]^{2+}$ cation, which are interconnected to propagate an intriguing two-dimensional (2D) network.

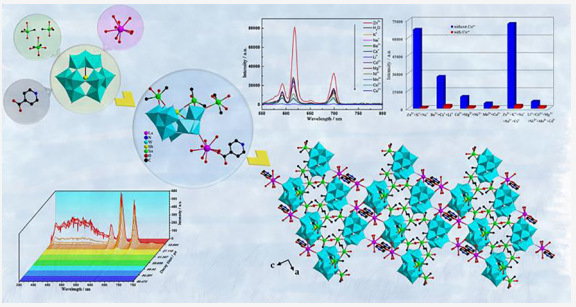

For all we know, **1**−**6** stand for the first 2D OT−Ln heterometallic polyoxometalates. Furthermore, luminescence performances of solid-state **3**−**6** were deeply surveyed at ambient temperature. Energy migration from $[B\text{-}\beta\text{-}SbW_9O_{33}]^{9-}$ and pca^- to Sm^{3+} centers in **5** was also studied. Comparative studies demonstrate that the contribution of $[B\text{-}\beta\text{-}SbW_9O_{33}]^{9-}$ sensitizing the emission of Sm^{3+} is prominently larger than that of pca^- sensitizing the emission of Sm^{3+} in the emission process of **5**. Most interestingly, **6** as a fluorescence probe exhibits high selectability and sensitivity for recognizing Zn^{2+} and Cu^{2+} in water.

INTRODUCTION

Tremendous progress on functional polyoxometalates (POMs) has been made in more recent decades because of their unique molecular compositions, diversified sizes and shapes, controllable acidity and charge density, and excellent redox capability, which lead to their unparalleled structural topologies and versatilities in catalytic, optical, electrochemical, magnetic, and medicinal properties.[1−6] Within this field, continuous exploration and discovery on organometal (OM)-decorated POMs have been painstakingly performed in recent years because of their synergistic functions between OM components and POM units. Thus, some OM components, such as organotitanium,[7,8] organoruthenium,[9,10] organorhodium,[11] organogermanium,[12] organotin (OT),[13−21] and organoantimony,[22] have been introduced to the POM system, leading to novel organic−inorganic hybrid OM-decorated POMs. Especially, OT-decorated POMs have drawn great concern thanks to the Sn−C good stability in aqueous solution and comparable radii between Sn^{IV} and W^{VI} centers, which are conducive to the incorporation of OT groups into the POM skeletons.[23,24] In 1979, Knoth and co-workers reported the first OT-decorated POMs.[13] Afterward, Malacria et al. isolated a series of tin-embedded monovacant α_1- and α_2-Dawson phosphotungstate diastereomers by grafting the coupling chiral amines to unprecedented OT-substituted $[\alpha_1\text{-}P_2W_{17}O_{61}]^{10-}$ species.[25] Concomitantly, outstanding progress on OT-decorated POMs has been also made because multivacant POMs can provide well-defined vacant sites for the incorporation of many more OT groups into inorganic nucleophilic skeletons (some examples are shown in the Supporting Information).[26−31]

However, synthesis and exploration of OT−TM/Ln (TM = transition-metal) heterometallic POMs are only in their infancy. Hitherto, only some sporadic OT−TM heterometallic POMs (OTTMHPOMs) have been reported (some examples are demonstrated in Figure S1a−d).[32−35] Compared with OTTMHPOMs, exploration and investigation on OT−Ln heterometallic POMs (OTLnHPOMs) are relatively laggard because of the fact that Ln^{3+} ions possess a strong oxytropic ability for highly negative POM entities, often producing amorphous sediments, which results in some difficulties in obtaining their single crystals.[36,37] Therefore, it is extremely challenging to develop suitable reaction strategies for synthesizing OTLnHPOMs. However, it is well-known that Ln-incorporated POMs are of considerable interest because of their remarkable properties in luminescence, Lewis acid

Received: March 13, 2020
Published: August 5, 2020

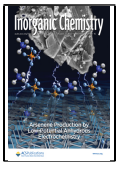

https://dx.doi.org/10.1021/acs.inorgchem.0c00768
Inorg. Chem. 2020, 59, 11287−11297

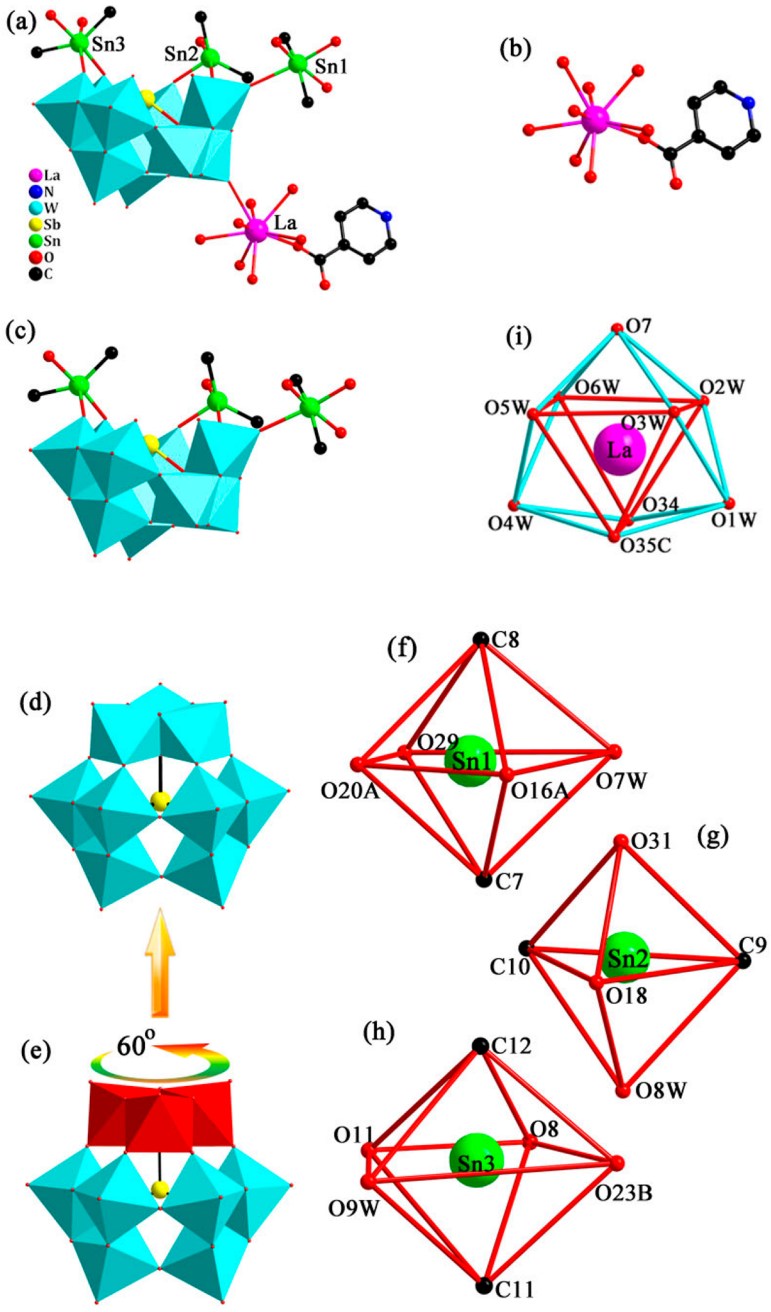

Figure 1. (a) Molecular moiety of **1**. (b) $[La(H_2O)_6(pca)]^{2+}$ cation. (c) B-β-SbW_9 segment stabilized by three $[Sn(CH_3)_2(H_2O)]^{2+}$ groups. (d) B-β-SbW_9 segment in **1**. (e) B-α-SbW_9 precursor. (f–h) Coordination geometries of $[Sn1(CH_3)_2(H_2O)]^{2+}$, $[Sn2(CH_3)_2(H_2O)]^{2+}$, and $[Sn3(CH_3)_2(H_2O)]^{2+}$ ions. (i) Monocapped square antiprism of the $[La(H_2O)_6(pca)]^{2+}$ ion. Symmetry codes: A, $-x$, $1-y$, $-z$; B, $1+x$, y, z; C, $-1-x$, $1-y$, $1-z$.

catalysis, electrochemistry, and magnetism.[38−43] Under this background, we began to explore this field. Through persistent efforts, very recently, our group has successfully synthesized two series of OTLnHPOMs with discrete structures by a facile synthetic method based on simple reactants in the assistance of organic solubilizers (here is dimethylamine hydrochloride), including the first OT−Ln heterometallic tellurotungstates (Figure S1e) and tetrameric *S*-shaped OTLnHPOMs (Figure S1f).[44,45] However, up to now, no OTLnHPOM with high-dimensional structure has been reported. With the aim of obtaining novel and high-dimensional OTLnHPOMs with interesting properties, we have actively exploited the reactivity among trilacunary precursors $[B\text{-}\alpha\text{-}SbW_9O_{33}]^{9-}$, B-$\alpha$-$SbW_9$, $(CH_3)_2SnCl_2$, and $Ln(NO_3)_3{\cdot}6H_2O$ and pyridine-4-carboxylic acid (Hpca) under acidic conditions by the step-by-step synthesis strategy considered in the following: (1) We used B-α-SbW_9 as a starting material because it is able to serve as a template agent to the direct aggregation of Ln^{3+} and $[(CH_3)_2Sn]^{2+}$ cations surrounding it, which offers the indispensable precondition for the constructiion of multi-dimensional structures. (2) Hpca not only has multifunctional N and O binding positions and can work as an excellent linker to coordinate with different metal centers but also functions as a solubilizing agent to partly enhance the dissolvability of Ln^{3+}

https://dx.doi.org/10.1021/acs.inorgchem.0c00768
Inorg. Chem. 2020, 59, 11287−11297

groups during the reaction, effectively improving the reactivity of Ln^{3+}, $[(CH_3)_2Sn]^{2+}$, and B-α-SbW_9 components and, to a certain extent, decreasing the rapid integration of B-α-SbW_9 precursors with highly oxophilic Ln^{3+} ions further to prevent the formation of amorphous precipitates. (3) We chose an acidic water medium because it not only makes for the dissolution of $(CH_3)_2SnCl_2$ and $Ln(NO_3)_3{\cdot}6H_2O$ but also can inhibit the hydrolysis of $[(CH_3)_2Sn]^{2+}$ and Ln^{3+} ions and reduce the precipitation of $[(CH_3)_2Sn]^{2+}$ and Ln^{3+} ions, which is conducive to the establishment of multidimensional structures of desired outcomes. Finally, we succeeded in obtaining a series of OT−Ln heterometallic antimotungstate (AMT) hybrids $[Ln(H_2O)_6(pca)]H[Sn(CH_3)_2(H_2O)]_3[B\text{-}\beta\text{-}SbW_9O_{33}]{\cdot}12H_2O$ [Ln = La^{3+} (**1**), Ce^{3+} (**2**), Pr^{3+} (**3**), Nd^{3+} (**4**), Sm^{3+} (**5**), Eu^{3+} (**6**)]. Notably, the molecular units of **1**−**6** are assembled from a trivacant B-β-SbW_9 segment stabilized by three $[Sn(CH_3)_2(H_2O)]^{2+}$ functionalized groups and a supporting $[Ln(H_2O)_6(pca)]^{2+}$ linker, and adjacent structural units are interconnected, propagating an intriguing two-dimensional (2D) network structure. For all we know, **1**−**6** not only stand for the first examples of OT−Ln heterometallic AMTs but also represent unprecedented 2D network OT−Ln heterometallic POMs. Investigations on the fluorescence (FL) and lifetime decay (LD) of **3**−**6** were systematically lucubrated. Furthermore, **6** can work as one fluorescent probe and exhibits benign selective power and sensitivity toward the detection of Cu^{2+} and Zn^{2+} in water.

RESULTS AND DISCUSSION

Structure Depiction. The high purity of **1**−**6** was verifed via powder X-ray diffraaction measurements (Figure S2). Single-crystal X-ray diffraaction analytical results reveal that **1**−**6** belong to the triclinic space group $P\bar{1}$ (Table S1). Herein, only the structural depiction of **1** is expounded. Its asymmetric unit (Figure 1a) is constituted by a trivacant B-β-SbW_9 segment, three $[Sn(CH_3)_2(H_2O)]^{2+}$ cations, a $[La(H_2O)_6(pca)]^{2+}$ cation (Figure 1b), and 12 H_2O molecules of crystallization. According to the charge-balance rule, one proton is needed in the structural formula. To determine the probable proton-bonding positions of **1**, we calculated the bond valence sum (BVS) values of the Sb, Sn, W, and La elements.[46] The results demonstrate that the Sb, Sn, W, and La centers in **1** are in their formal valences of 3+, 4+, 6+, and 3+, respectively. The BVS value of 1.65 for O30 connecting with W5 is obviously less than 2 (Table S2), manifesting the possible monoprotonation position. It should be noted that three $[Sn(CH_3)_2(H_2O)]^{2+}$ groups are implanted in the trivacant positions of B-β-SbW_9 and stabilize the structure of B-β-SbW_9 (Figure 1c). The Sb^{III} heteroatom in B-β-SbW_9 (Figure 1d) exhibits a trigonal-pyramidal geometry determined by triple μ_4-O atoms from three $\{W_3O_{13}\}$ trimers [Sb−O, 1.977(6)−2.004(7) Å] (Table S3), and every $\{W_3O_{13}\}$ trimer is established by three edge-sharing $\{WO_6\}$ groups [W−O, 1.709(7)−2.359(6) Å]. Intriguingly, the emergence of B-β-SbW_9 reveals that B-α-SbW_9 (Figure 1e) → B-β-SbW_9 has happened in the formation of **1** because B-α → B-β isomerization of the SbW_9 segment is facilitated in an acidic aqueous solution,[47] which agrees well with the synthetic conditions of **1** (pH = 3.2). Such a phenomenon has previously been observed.[26,47−49] More appealingly, three crystallographically unique $[Sn(CH_3)_2(H_2O)]^{2+}$ cations in **1** jointly bond to the B-β-SbW_9 fragment but possess disparate coordination geometries. The $[Sn1(CH_3)_2(H_2O)]^{2+}$ group resides in the six-coordinated contorted octahedron constructed from a terminal O (O29) in one B-β-SbW_9 [Sn−O, 2.372(7) Å], two lacunary O atoms (O16A and O20A) in the other B-β-SbW_9 [Sn−O, 2.054(7)−2.125(7) Å], two methyl C atoms (C7 and C8) [Sn−C, 2.102(13)−2.104(13) Å], and one H_2O molecule (O7W) [Sn−O, 2.574(7) Å] (Figure 1f). The $[Sn2(CH_3)_2(H_2O)]^{2+}$ group is five-coordinated and displays a contorted trigonal bipyramid established by two lacunary O atoms (O18 and O31) from two $\{W_3O_{13}\}$ trimers in the B-β-SbW_9 segment [Sn−O, 1.999(8)−2.086(7) Å], two methyl C atoms (C9 and C10) [Sn−C, 2.088(14)−2.106(14) Å], and a O8W ligand [Sn−O, 2.323(9) Å] (Figure 1g). Similar to the $[Sn1(CH_3)_2(H_2O)]^{2+}$ group, the $[Sn3(CH_3)_2(H_2O)]^{2+}$ group displays the octahedral configuration, where the equatorial positions are taken up by two lacunary O atoms (O8 and O11) provided by one B-β-SbW_9 [Sn−O, 2.070(7)−2.076(13) Å], one terminal O atom (O23B) provided by the other B-β-SbW_9 [Sn−O, 2.378(7) Å], two methyl C atoms (C11 and C12) [Sn−C, 2.088(13)−2.095(7) Å], and an H_2O molecule (O9W) [Sn−O, 2.594(7) Å] (Figure 1h). Close inspection of **1** demonstrates that ∠C−Sn1−C angles are apparently lower than 180° (∠C−Sn1−C, 156.8(6) Å; ∠C−Sn2−C, 133.7(7) Å; ∠C−Sn3−C, 148.1(6) Å), suggesting the existence of repulsive interaction among methyl groups. It is noteworthy that a similar grafted fashion of dimethyltin groups in the B-β-SbW_9 moiety has been previously observed in $[\{Sn(CH_3)_2\}_3(H_2O)_4(\beta\text{-}XW_9O_{33})]^{3-}$ (X = As^{III}, Sb^{III}) in 2004.[26] In **1**, the nine-coordinated twisted tricapped trigonal prism of La^{3+} is made up of a O7 atom of one B-β-SbW_9, one carboxylic O34 atom of the pca^- ligand, one carboxylic O35C atom from the other $[La(H_2O)_6(pca)]^{2+}$ linker, and six H_2O ligands (O1W−O6W; Figure 1i) [La−O, 2.441(8)−2.627(10) Å; ∠O−La−O, 64.5(4)−144.4(3)°]. Furthermore, the $[La(H_2O)_6(pca)]^{2+}$ group not only grafts to one side of the B-β-SbW_9 fragment via the terminal O7 atom but also provides the precondition for deriving the extended structure of **1**.

Interestingly, further inspection of **1** shows that two adjacent asymmetric $\{[La(H_2O)_6(pca)][Sn(CH_3)_2(H_2O)]_3[B\text{-}\beta\text{-}SbW_9O_{33}]\}^-$ units can be connected together in a staggered fashion by the bridging $[Sn1(CH_3)_2(H_2O)]^{2+}$ linkers, creating the centrosymmetric dimeric $\{\{[La(H_2O)_6(pca)][Sn(CH_3)_2(H_2O)]_3[B\text{-}\beta\text{-}SbW_9O_{33}]\}_2\}^{2-}$ entity [Sn−O, 2.125(7)−2.372(7) Å; ∠O−Sn−O, 168.6(3)°] (Figure 2a,b). Then adjacent dimeric $\{\{[La(H_2O)_6(pca)][Sn(CH_3)_2(H_2O)]_3[B\text{-}\beta\text{-}SbW_9O_{33}]\}_2\}^{2-}$ entities can be further interconnected through dimeric $\{\{[La(H_2O)_6(pca)]\}_2\}^{4+}$ connectors, propagating a one-dimensional (1D) zigzag chain (Figure 2c). Furthermore, adjoining 1D zigzag chains can be concatenated to each other by $[Sn3(CH_3)_2(H_2O)]^{2+}$ linkers to propagate an unusual 2D wavelike sheet architecture in the ac plane (Figure 2d). Notably, from the stacking alignment along the *a*-axis we can also see that neighboring 2-D wave-like sheets regularly parallel with each other, creating the three-dimensional (3D) stacking alignment of **1** (Figure 3a). Figure 3b presents the simplified 2D stacking alignment of **1**. For all we know, this alluring structure has first been observed within OTLnHPOMs, representing a rare example of a POM fragment concurrently including Ln^{3+} cations, OT groups, and pyridinecarboxylate ligands with respect to those only comprising OT or Ln^{3+} components or both with isolated structures.[25−31,44,45]

FL Studies. Owing to the particular electron-structure features of Ln^{3+} ions, Ln^{3+}-included compounds have aroused

https://dx.doi.org/10.1021/acs.inorgchem.0c00768
Inorg. Chem. 2020, 59, 11287−11297

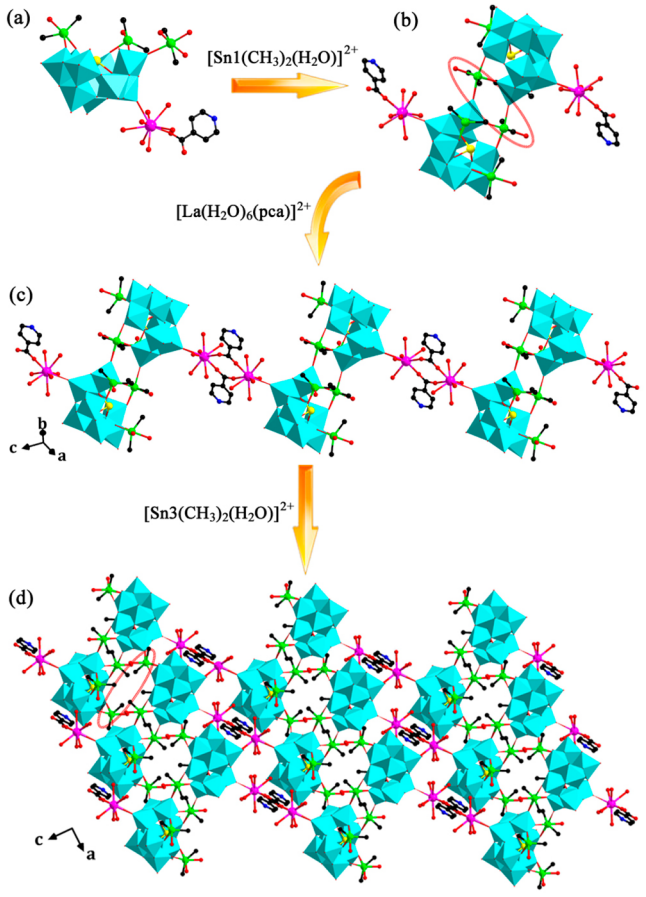

Figure 2. (a) Asymmetric molecular moiety of **1**. (b) Centrosymmetric dimeric $\{[La(H_2O)_6(pca)][Sn(CH_3)_2(H_2O)]_3[B\text{-}\beta\text{-}SbW_9O_{33}]\}_2^{2-}$ entity. (c) 1D zigzag chainlike structure in the *ac* plane. (d) 2D wavelike sheet of **1** in the *ac* plane.

sustained attraction in biomedical sensory probe lasers, kinescopes, projected displays, and plasma displays.[50−57] Herein, FL investigations on **3**−**6** in the solid state were deeply made at ambient temperature. Among them, FL studies of **3**−**5** were discussed in the Supporting Information.

When **6** was excited by a radiation of 394 nm, the UV−vis emission spectrum (ESS) of **6** reveals the Eu^{3+} luminescence peaks at 579, 593, 613, 617, 650, and 699 nm, respectively (Figure 4a). The most intense emission (ES) peak at 613 nm accompanied by a splitting peak at 617 nm corresponds to the Eu^{3+5} $D_0 \rightarrow {}^7F_2$ transition, whereas those peaks centered at 579, 593, 650, and 699 nm are severally ascribed as ${}^5D_0 \rightarrow {}^7F_J$ (J = 0, 1, 3, 4) transitions.[58] Although the symmetric-forbidden ${}^5D_0 \rightarrow {}^7F_0$ ES intensity at 579 nm is very feeble, its emergence indicates the low symmetrical circumstances of Eu^{3+} in **6**,[59] which coincides with the structure analytical conclusion. Formally, the MD ${}^5D_0 \rightarrow {}^7F_1$ ES intensity is insensitive to the ligand-field intensity in the surrounding of Eu^{3+}, while the ED ${}^5D_0 \rightarrow {}^7F_2$ ES intensity is susceptive to the ligand-field intensity in the surroundings of Eu^{3+}.[60] The MD ${}^5D_0 \rightarrow {}^7F_1$ ES is predominant in the symmetrical surroundings, whereas the ED ${}^5D_0 \rightarrow {}^7F_2$ ES is preponderant in the case of asymmetry.[61,62] Hence, the $I({}^5D_0 \rightarrow {}^7F_2)/I({}^5D_0 \rightarrow {}^7F_1)$ percentage is normally viewed as an indicator to inspect the partial symmetry of Eu^{3+}. For **6**, the percentage is ca. 5.6, which testifies to the low symmetrical circumstances of Eu^{3+}. The ECS of **6** (Figure S12) monitored by the ES intensity at 613 nm displays four Eu^{3+} distinctive ES peaks at 362 nm (${}^7F_0 \rightarrow {}^5D_4$), 376−385 nm (${}^7F_0 \rightarrow {}^5G_3$), 394 nm (${}^7F_0 \rightarrow {}^5L_6$), and 417 nm (${}^7F_0 \rightarrow {}^5D_3$). In addition, the LD curve of **6** (Figure S5b), measured by supervising the 613 nm ES peak, adheres to the monoexponential equation, yielding the FL lifetime τ of 173.00 μs and the agreement coefficient χ^2 of 1.062. Its longevity becomes short in comparison with $K_{13}[Eu(SiW_{11}O_{39})_2]$ (2.440 ms) and $Na_{0.5}Cs_{4.5}[Eu(\alpha\text{-}SiW_{11}O_{39})(H_2O)_2]\cdot 23H_2O$ (0.39 ms).[63] Stick out a mile, six H_2O ligands coordinate to each Eu^{3+} in **6**, each Eu^{3+} in $K_{13}[Eu(SiW_{11}O_{39})_2]$ links to eight O atoms from two $[\alpha\text{-}SiW_{11}O_{39}]^{8-}$ moieties but without H_2O ligands, and each Eu^{3+} in $Na_{0.5}Cs_{4.5}[Eu(\alpha\text{-}SiW_{11}O_{39})(H_2O)_2]\cdot 23H_2O$ is combined with two H_2O ligands. As a result, the reason for this phenomenon is principally because the high-frequency oscillating O−H groups in H_2O molecules on Eu^{3+} in **6** are capable of quenching the ES behavior by nonradiative inactivation of the ${}^5D_0$ state.[64] Moreover, the LD curve of **6** adheres to the monoexponential equation, while the LD profile of **5** fits to a biexponential equation. We speculate that this is because the lifetimes of B-β-SbW_9 and pca^- are negligible compared with the long FL lifetime of Eu^{3+}. Eventually, the ESS of **6** excited by the 285 nm irradiation was collected and exhibited no additional peak within the scope of 400−550 nm (Figure 4b). Time-resolved emission spectroscopy (TRES) profiles of **6** in the ES range of 350−750 nm were also recorded upon irradiation of 285 nm (Figure 4c), which display that the ES intensities of B-β-SbW_9 and pca^- only appear in the beginning (Figure S13) and are almost negligible in the ES of **6**. However, the appearance of the ES intensity of B-β-SbW_9 and pca^- in the beginning in the TRES profiles of **6** may manifest the occurrence of slight electron transfer (ET) from B-β-SbW_9 and pca^- to Eu^{3+}. To probe the contributions of B-β-SbW_9 and pca^- sensitizing the ES of Eu^{3+}, comparative experiments on the ESS of the solution of $Eu(NO_3)_3\cdot 6H_2O$, the mixed solution of $Eu(NO_3)_3\cdot 6H_2O$ and Hpca, the mixed solution of $Eu(NO_3)\cdot 6H_2O$ and SbW_9, and the mixed solution of $Eu(NO_3)_3\cdot 6H_2O$, Hpca, and SbW_9 have also been measured under 285 nm excitation in water under similar conditions (Figure S14). Similar to **5**, the introduction of Hpca leads to the very feeble increase of the ES intensity of $Eu(NO_3)_3\cdot 6H_2O$. When SbW_9 was introduced, the rise of the ES intensity of $Eu(NO_3)_3\cdot 6H_2O$ was apparent. Upon further introduction of Hpca to the $Eu(NO_3)_3\cdot 6H_2O$ + SbW_9 system, the ES intensity of the system changes a little. What is s interesting is that whether the solution was excited by a radiation of 285 or 394 nm (Figure S15), the trends of the ES intensity of the solution are similar. This results also verifies that the contribution of B-β-SbW_9 sensitizing the ES of Eu^{3+} is noteworthily bigger than that of pca^- sensitizing the ES of Eu^{3+} in the ES process of **6**.

Sensing of Metal Ions. Detecting trace metal ions has captured increasing interest because the excess metal ions can bring about various diseases of organisms.[65,66] To date, numerous luminescent materials of Ln-based compounds (LnBCs), especially metal−organic frameworks (MOFs), have been resoundingly used to detect metal ions.[67,68] Nevertheless, manufacturing Ln-POM sensors owning quick response and high agility to detect metal ions still remains a fascinating subject of study. According to previously reported literatures, the preferred coordination of Eu^{3+} cations toward carboxylic O atoms over pyridinyl N atoms in **6** likely benefits free Lewis basic pyridinyl N atoms to coordinate with metal ions, which means that **6** may be a promising candidate as a FL sensor. As a result, we were determined to explore its possible

https://dx.doi.org/10.1021/acs.inorgchem.0c00768
Inorg. Chem. 2020, 59, 11287−11297

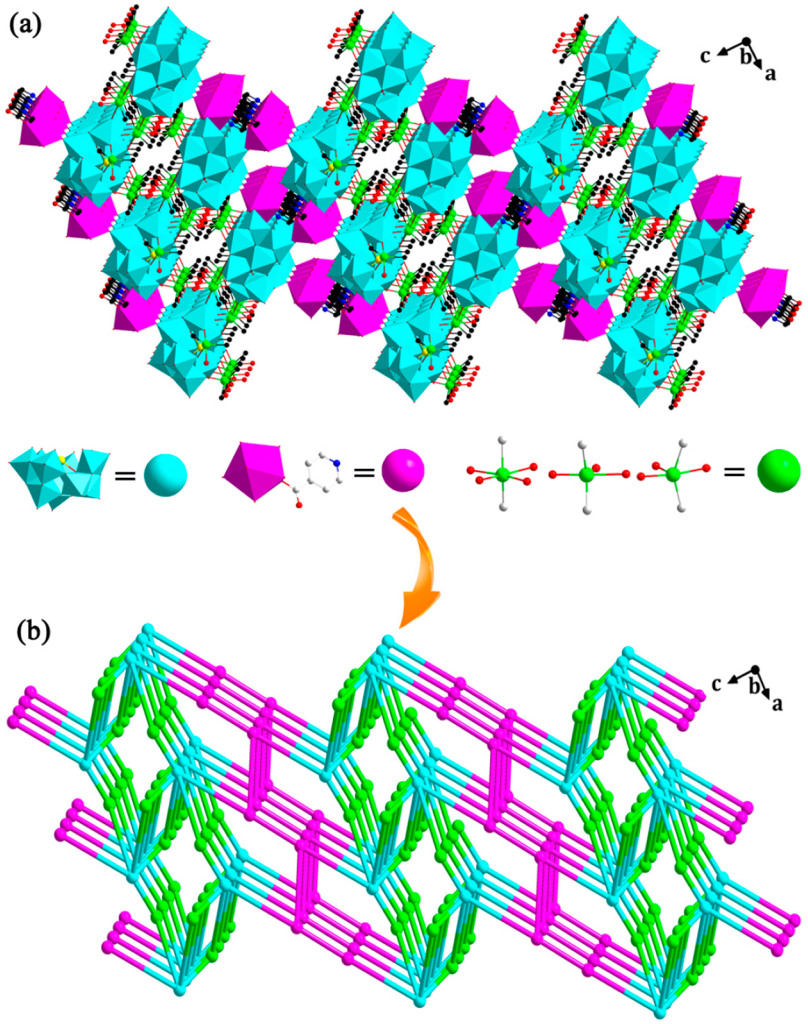

Figure 3. (a) 3D stacking structure of **1**. (b) Simplified 3D stacking topology of **1**.

application in the selective sensing of different metal cations based on the intense luminescence behavior of **6**.

To explore the recognition capability of **6** toward trace metal cations, we investigated the FL properties of **6** in water. We found that **6** was slightly soluble in water. Therefore, the ground **6** (5 mg) was dispersed in water (5 mL) and then treated by ultrasonication. The resulting suspension was centrifuged at a speed of 8000 rpm for 2 min. The supernate was used as the testing solution in the experiments of luminescence and UV studies. For the sake of investigating whether pH variation resulting from the introduction of different metal cations can influence the FL stability of **6** in aqueous environment, the effects of pH variation of an aqueous solution on the ES behavior of **6** were examined (the pH was adjusted by HCl or NaOH; Figure S17a,b). The results show that FL ESS of **6** dissolved in an aqueous solution exhibits good stability when the pH is varied from 2 to 8, suggesting that the polyoxoanion structure skeleton (PSS) of **6** may be retained in this process. Moreover, UV spectra of **6** dissolved in water under different pH values (adjusted by HCl or NaOH) were also explored by (200−400 nm), which can confirm that the PSS of **6** dissolved in an aqueous solution may be stable in pH = 3−8 (Figure S18). In order to affirm whether the PSS of **6** exists or not in water, electrospray ionization mass spectrometry (MS) of **6** (Figure S19) in water under pH values ranging from 1 to 12 was also carried out at ambient temperature, and we could explicitly observe that the main MS signal (at about m/z 916.37) bearing a negative charge of 3− always exists when the pH value varies from 2 to 8, which can be approximately assigned to the $[H_2Eu(pca)Sn(CH_3)_2(H_2O)(SbW_9O_{33})]^{3-}$ fragment. This result indicates that the PSS of **6** is basically maintained in water except that two $[Sn(CH_3)_2(H_2O)]^{2+}$ cations and all of the coordinated H_2O molecules on the Eu^{3+} ion are dissociated from the structural unit. Apparently, the dissociation of two $[Sn(CH_3)_2(H_2O)]^{2+}$ cations from the structural unit of **6** leads to destruction of the 2D structure in water; however, the basic maintainance of the PSS of **6** in water of pH = 2−8 reveals that **6** can still serve as a FL sensor candidate. Thus, we studied the recognition properties of **6** toward different metal cations in water at ambient temperature. Correspondingly, the recognition experiments of metal cations were performed. The grated sample of **6** (5 mg) was suspended in 5 mL of disparate distilled water solutions containing 1×10^{-2} mol L^{-1} MCl_x (M = Zn^{2+}, K^+, Na^+, Ba^{2+}, Cs^+, Li^+, Cd^{2+}, Mg^{2+}, Ni^{2+}, Mn^{2+}, Co^{2+}, Cu^{2+}) and treated with care for luminescence studies. It could be observed from Figure S20a,b that various metal ions reveal prominently diverse influences on the ES intensities of **6**. Obviously, the ES intensity at 613 nm in the existence of Zn^{2+} is enhanced about three times compared to the case without

https://dx.doi.org/10.1021/acs.inorgchem.0c00768
Inorg. Chem. 2020, 59, 11287−11297

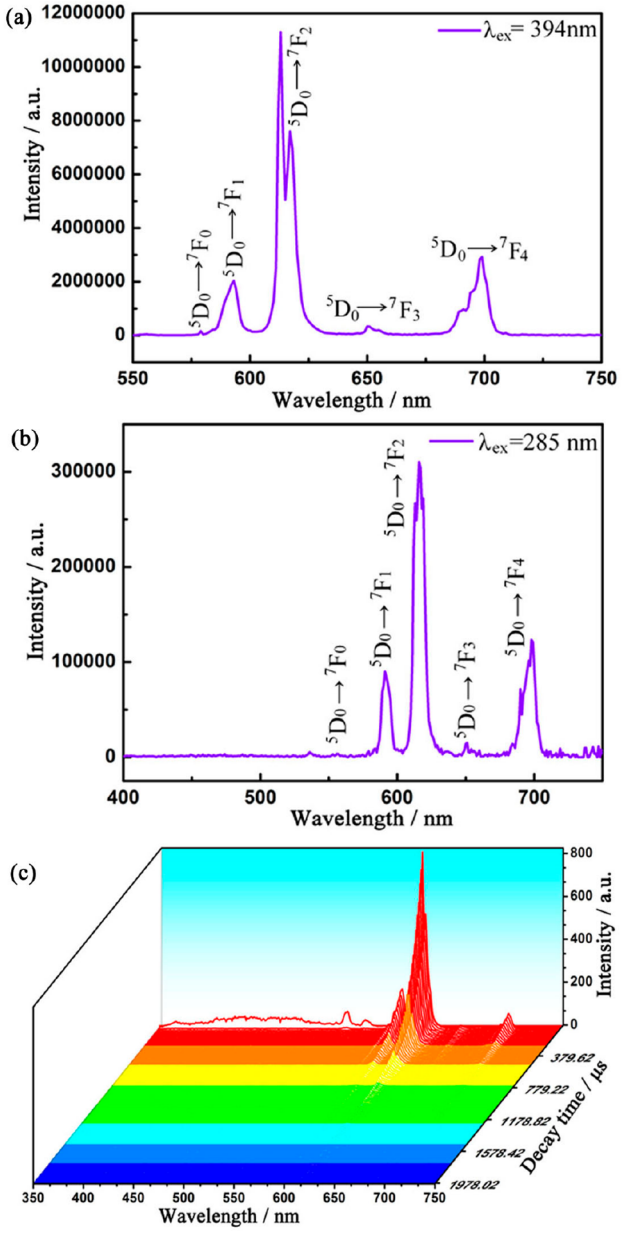

Figure 4. (a) ESS of **6** excited by 394 nm light. (b) ESS of **6** excited the 285 nm light. (c) TRES patterns of **6**.

Zn^{2+}. In contrast, the ESS with Cu^{2+} shows apparent FL quenching, and the ES strength quickly decreases from 28900 to 795 au in comparison with the case without Cu^{2+} [QP (quenching percentage) = $1 - I/I_0$ = 97.2%, where I and I_0 denote the FL intensities of **6** before and after the addition of Cu^{2+}]. The rest of the metal cations display a negligible impact (KCl, NaCl, $BaCl_2$, CsCl, LiCl, and $CdCl_2$) or a small degree of quenching effect ($MgCl_2$, $NiCl_2$, $MnCl_2$, and $CoCl_2$) on the luminescence of **6**. Additionally, the LD curves were also measured to further research influences of the Zn^{2+} FL enhancement impact and the Cu^{2+} FL quenching impact on the ES behavior of **6** (Figure S21). Figures S21a and S16m show that the ES lifetime of **6** significantly increases from 159.06 to 235.71 μs in the presence of Zn^{2+} and decreases from 159.06 to 14.44 μs in the emergence of Cu^{2+}, which coincides with their ES test results. Influences of other metal cations on the lifetime of **6** were also shown in Figure S19b–l, which have a slight or negligible effect on the FL lifetime of **6**. Furthermore, we investigated the effects of different anions (including Cl^-, Br^-, SO_4^{2-}, $CH_3$and COO^-) on the FL intensity of **6**, which shows that these anions have negligible interference during the detection of Zn^{2+} or Cu^{2+} (Figure S22). The cases imply that **6** has a high selectivity for recognizing Zn^{2+} and Cu^{2+} in an aqueous solution and can be used as a luminescent probe.

Apart from assessing the strong sensitivity, the antijamming capability of **6** as a sensor is also essential. Thus, the influences of other metal ions on the detection of Zn^{2+} or Cu^{2+} were also detected. While the other metal-ion concentration was maintained at 1×10^{-2} mol L^{-1} in water, the same Zn^{2+} or Cu^{2+} concentration was then introduced. The results show the ES strength of **6** as a sensor for monitoring Zn^{2+} is almost impervious to alkali- and alkaline-earth-metal ions (K^+, Na^+, Cs^+, Li^+, Ba^{2+}, and Mg^{2+}) or Cd^{2+} but is easily disturbed by Ni^{2+}, Mn^{2+}, Co^{2+}, and Cu^{2+} (Figure S23). However, Cu^{2+} could still induce a drastic FL decrease even in the coexistence of two, three, five, or six kinds of other metal ions (Figure S20c,d). Adequate experimental results further prove the high selectivity of **6** toward the Cu^{2+} recognition.

Meanwhile, we have also performed related FL titration experiments, and the FL intensities of **6** have been measured by the addition of varying Cu^{2+} or Zn^{2+} concentrations in solutions of **6**. As demonstrated in Figure 5a, the FL strength of **6** decreases with increasing Cu^{2+} concentration, and the FL strength of **6** is almost completely quenched when the Cu^{2+} concentration reaches to 8.0×10^{-3} mol L^{-1} (Figure 5a). The relationship of the quenching FL strength and Cu^{2+} concentration in the range of $(0–9.6) \times 10^{-4}$ mol L^{-1} (Figure 5b) could be well fitted through the Stern–Volmer function: $I_0/I = 1 + K_{SV}[C]$,[69,70] where K_{SV} stands for a quenching constant and [C] represents the concentration of a metal ion, giving a linearly dependent coefficient (R^2) of 0.9783 and K_{SV} of 4.585×10^3 mol^{-1} L for Cu^{2+}, which is far higher than those of the MOFs for sensing Cu^{2+} (Table S4),[71−77] demonstrating its obvious luminescent quenching toward **6**. With respect to Zn^{2+}, the ES intensity of **6** is enhanced with increasing Zn^{2+} concentration between 0 and 0.024 mol L^{-1} and does not induce a concentration quenching effect (CQE) of the FL signal (Figure 5c). Correspondingly, the ES lifetime of **6** dramatically increases from 159.06 to 342.03 μs (Figure S24). However, upon further elevation of the Zn^{2+} concentration, the CQE occurs (Figure S25). Quantitatively, this FL enhancement effect of **6** with the concentration of Zn^{2+} varying from 0 to 0.024 mol L^{-1} could also be simulated through the Stern–Volmer function: $I/I_0 = 1 + K_{SV}^*[C]$,[78] in which K_{SV}^* denotes an enhancement constant, affording R^2 of 0.9747 (Figure 5d) and K_{SV}^* of 3.825×10^2 mol^{-1} L for Zn^{2+}.

Besides, in order to further probe the contribution of AMT components during the metal-ion recognition of **6**, comparative experiments of $Eu(NO_3)_3{\cdot}6H_2O$ as a FL sensor in the same molar concentration to **6** to the sensing of 1×10^{-2} mol L^{-1} MCl_x metal cations (M = Zn^{2+}, Na^+, Ba^{2+}, Li^+, Cd^{2+}, and Cu^{2+}) in water were studied by ESS. As demonstrated in Figure S26, however, we could not see any characteristic peaks of Eu^{3+} in the ESS of $Eu(NO_3)_3{\cdot}6H_2O$. As a result, we studied the recognition experiments of $Eu(NO_3)_3{\cdot}6H_2O$ in the same mass concentration to **6** for detection of these different metal ions. In Figure S27, the characteristic ES intensity of $Eu(NO_3)_3{\cdot}6H_2O$ in the existence of these metal ions does not show an obvious change in comparison with the case only

https://dx.doi.org/10.1021/acs.inorgchem.0c00768
Inorg. Chem. 2020, 59, 11287−11297

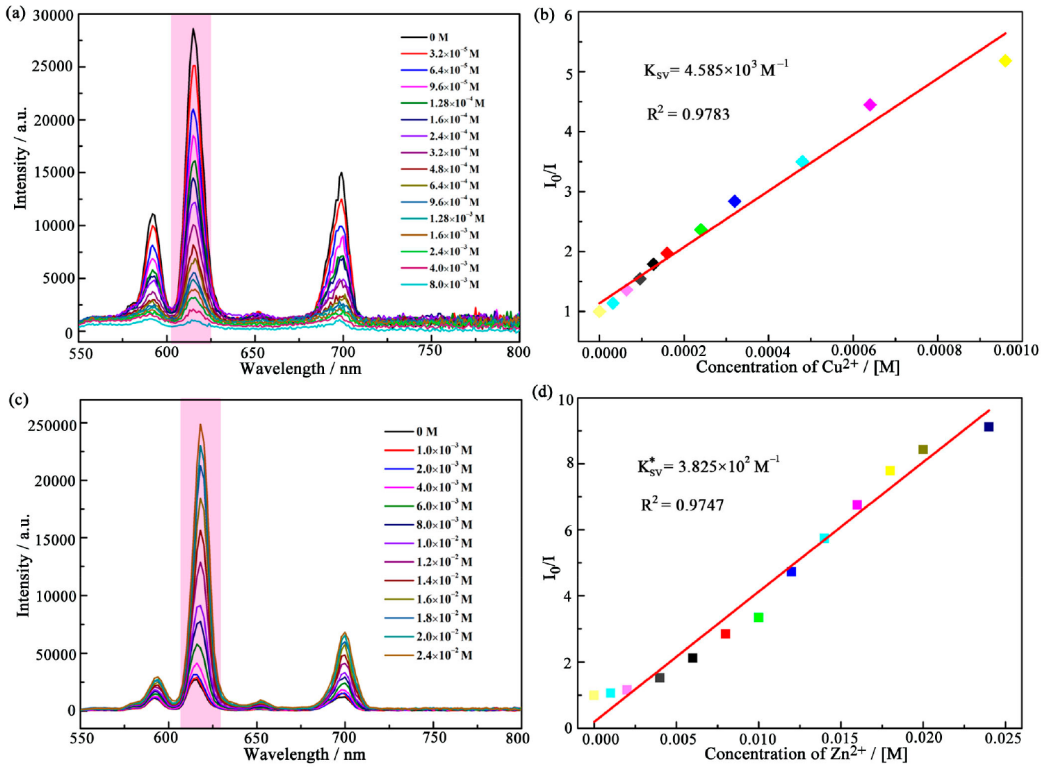

Figure 5. (a) Variation of the ESS of **6** dissolved in aqueous solution with enhancement of the Cu^{2+} concentration. (b) Plot of the ES strength of the 613 nm peak and the Cu^{2+} concentration and its linear fitting result. (c) Variation of the ESS of **6** dissolved in an aqueous solution with increasing Zn^{2+} concentration. (d) Plot of the ES strength of the 613 nm peak and the Zn^{2+} concentration and its linear fitting result.

in the existence of $Eu(NO_3)_3{\cdot}6H_2O$, which illuminates that AMT components in **6** make a vital contribution to the detection of metal ions and also proves that the contribution of B-β-SbW_9 sensitizing the ES of Eu^{3+} is nonnegligible in the detection procedure.

Finally, the possible FL recognition mechanisms were diligently investigated. IR spectra of undissolved **6** after immersion in aqueous solutions with various metal ions were measured, which shows that the PSS of **6** remains unchanged (Figure S28), indicating that the enhancement influence of Zn^{2+} and the quenching influence of Cu^{2+} on the FL of **6** could not be assigned to collapse of the PSS. Moreover, UV spectra of metal ions of MCl_x (M = Zn^{2+}, K^+, Na^+, Ba^{2+}, Cs^+, Li^+, Cd^{2+}, Mg^{2+}, Ni^{2+}, Mn^{2+}, Co^{2+}, Cu^{2+}) in an aqueous solution have been investigated (Figure S29). It is obvious that the UV absorption bands of all of the metal ions except Cu^{2+} are lower than 200 nm. For Cu^{2+}, an obvious absorption band can be seen in the range of 190−250 nm (Figure S29l), which partially overlaps with the UV absorption peak of SbW_9 and Hpca (200−315 nm). This observation demonstrates that Cu^{2+} competes for obvious photon absorption with B-β-SbW_9 and pca^- in the EC procedure, which can result in a decrease of the FL intensity of **6**. In addition, the preferred coordination of the Eu^{3+} ion to carboxylic O atoms over pyridinyl N atoms in **6** can likely be beneficial to free Lewis basic pyridinyl N atoms to coordinate with metal ions. Therefore, **6** can also exhibit different recognition performances toward different metal cations: K^+, Na^+, Ba^{2+}, Cs^+, and Li^+ ions have very weak binding interactions with carboxylic O and pyridinyl N atoms, and their influence on the ES of the Eu^{3+} ion can be negligible, whereas Co^{2+}, especially Cu^{2+}, can strongly bind with carboxylic O and pyridinyl N atoms, leading to significantly reduction of the ES of the Eu^{3+} ion. We speculate that strong binding interactions between Cu^{2+} with carboxylic O and pyridinyl N atoms of pca^- in **6**, which to some degree impairs the antenna effect of pca^- to sensitize Eu^{3+} f−f transitions, are similar to those observed in the reported literatures.[81,82] It can be concluded that both the larger competitive photon absorption of Cu^{2+} than those of B-β-SbW_9 and pca^- and strong binding interactions between Cu^{2+} and carboxylic O and pyridinyl N atoms of pca^- can quench the ES of the Eu^{3+} ion in **6**, leading to the sensing property of **6** toward Cu^{2+}. For the FL enhancement mechanism of Zn^{2+}, we assume that the increase of the ESS intensity of **6** may be related to the case that coordination of Zn^{2+} with pca^- produces enhanced ET from pca^- to Eu^{3+} in the sensing process; thus, relative comparative experiments on the ESS of Hpca and a mixture of Hpca and Zn^{2+} have also been measured under the 394 nm excitation in water with the same proportions to the metal-ion recognition experiments of **6** under similar conditions (Figure S30). As shown in Figure S30a, the characteristic peak in 400−600 nm of Hpca can indeed be observed. When $ZnCl_2$ was introduced, the ES intensity of the mixture of Hpca and Zn^{2+} exhibits a notable increase (Figure S30b), which suggests that the coordination of Zn^{2+} with Hpca can enhance the ES of Hpca. Thus, we can infer that the coordination of Zn^{2+} with pca^- through carboxylic O and pyridinyl N atoms results in the ES enhancement of pca^- during the sensing course of **6** toward Zn^{2+}. Apparently, the characteristic ES peak in 400−600 nm of pca^- partly overlaps with the Eu^{3+} EC peaks (Figure S12), manifesting that the characteristic ES of pca^- can be reabsorbed by Eu^{3+} in **6** and thus leading to the ES enhancement. This understanding is supported by the theory that FL resonance ET can enhance the FL emission.[79−84]

https://dx.doi.org/10.1021/acs.inorgchem.0c00768
Inorg. Chem. 2020, 59, 11287−11297

Additionally, as discussed above, B-β-SbW_9 plays a larger role in sensitizing the ES of Eu^{3+} than that of pca^- sensitizing the ES of Eu^{3+} in the ES process of **6**. In order to identify that B-β-SbW_9 also has the properties of **6** upon the recognition of metal ions, some comparative experiments have been made (Figures S31−S33). Comparisons of the ES intensity of the mixed solution of $Eu(NO_3)_3{\cdot}6H_2O$ and Hpca in the same mass concentration as **6** in water in the existence of diverse metal cations (M = Zn^{2+}, Na^+, Ba^{2+}, Li^+, Cd^{2+}, Cu^{2+}; 1×10^{-2} mol L^{-1}; λ_{ex} = 394 nm) reveal that the mixed solution of $Eu(NO_3)_3{\cdot}6H_2O$ and Hpca does not have recognition performance toward Zn^{2+} and Cu^{2+} in water (Figure S31). In order to identify the role of B-β-SbW_9 in the detection of Cu^{2+} and Zn^{2+} (1×10^{-2} mol L^{-1+}), comparative experiments of the ESS of $Eu(NO_3)_3{\cdot}6H_2O$, the mixed solution of $Eu(NO_3)_3{\cdot}6H_2O$ and $CuCl_2/ZnCl_2$, the mixed solution of $Eu(NO_3)_3{\cdot}6H_2O$, $CuCl_2/ZnCl_2$, and Hpca, the mixed solution of $Eu(NO_3)_3{\cdot}6H_2O$, $CuCl_2/ZnCl_2$, and SbW_9, and the mixed solution of $Eu(NO_3)_3{\cdot}6H_2O$, $CuCl_2/ZnCl_2$, SbW_9, and Hpca have been measured under 394 nm excitation in water under similar conditions. The comparison of Figures S32a−c and S33a−c illustrates that, in the absence of SbW_9, the ES intensity of $Eu(NO_3)_3{\cdot}6H_2O$ changes slightly when Cu^{2+}/Zn^{2+} and Hpca were introduced to the $Eu(NO_3)_3{\cdot}6H_2O$ system; however, the ES intensity of $Eu(NO_3)_3{\cdot}6H_2O$ after the introduction of SbW_9 (Figures S32d and S33d) indicates the FL quenching effect for the $Eu(NO_3)_3{\cdot}6H_2O$ + $CuCl_2$ + SbW_9 system and the FL enhancement effect for the $Eu(NO_3)_3{\cdot}6H_2O$ + $ZnCl_2$ + SbW_9 system. Upon a further introduction of Hpca to the $Eu(NO_3)_3{\cdot}6H_2O$ + $CuCl_2$ + SbW_9 system, the ES intensity of the system changes slightly (Figure S32e). When Hpca was further introduced to the $Eu(NO_3)_3{\cdot}6H_2O$ + $ZnCl_2$ + SbW_9 system, the ES intensity of the system was further enhanced (Figure S33e). These results display that B-β-SbW_9 in the system makes a great contribution during the detection of metal cations.

CONCLUSIONS

In this paper, we introduced Ln^{3+} ions, diorganotin groups, and organic ligands into the AMT precursor system, constructing six OT−Ln heterometallic AMT hybrids **1**−**6**, which represent the first 2D OTLnHPOMs. In-depth investigations on the FL and LD of **3**−**6** in the solid state were explored. Research results indicate ET from B-β-SbW_9 and pca^- to Sm^{3+} in **5**, and the contribution of $[B\text{-}\beta\text{-}SbW_9O_{33}]^{9-}$ sensitizing the emission of Sm^{3+} is prominently larger than that of pca^- sensitizing the emission of Sm^{3+} in the emission process of **5**. Above all, **6** as a FL probe exhibits good selectivity and sensitivity toward the recognition of Cu^{2+} and Zn^{2+}. This work not only is a major step forward in the preparation of OTLnHPOMs with extended structures but also is very promising because it taps into a currently rarely studied research field—POMs as ES sensors—and opens up a new perspective of developing FL probes of Ln-POM materials. The follow-up researches are going to be concentrated on several facets: (1) introducing selenotungstates/arsenotungstates/polyoxovanadates/polyoxoniobates to enrich the system of OTLnHPOMs; (2) introducing various poly(carboxylic acid) ligands or more than one kind of organic ligands at the same time to obtain high-dimensional OTLnHPOMs; (3) continuously developing optical, electrochemical, and catalytic applications of Ln-POMs.

ASSOCIATED CONTENT

Supporting Information

The Supporting Information is available free of charge at https://pubs.acs.org/doi/10.1021/acs.inorgchem.0c00768.

Experimental section, BVS results, relevant structure and FL figures, and IR and TG curves (PDF)

Accession Codes

CCDC 1990007−1990012 contain the supplementary crystallographic data for this paper. These data can be obtained free of charge via www.ccdc.cam.ac.uk/data_request/cif, or by emailing data_request@ccdc.cam.ac.uk, or by contacting The Cambridge Crystallographic Data Centre, 12 Union Road, Cambridge CB2 1EZ, UK; fax: +44 1223 336033.

AUTHOR INFORMATION

Corresponding Authors

Lijuan Chen − *Henan Key Laboratory of Polyoxometalate Chemistry, College of Chemistry and Chemical Engineering, Henan University, Kaifeng, Henan 475004, China*; Email: ljchen@henu.edu.cn

Junwei Zhao − *Henan Key Laboratory of Polyoxometalate Chemistry, College of Chemistry and Chemical Engineering, Henan University, Kaifeng, Henan 475004, China*; orcid.org/0000-0002-7685-1309; Email: zhaojunwei@henu.edu.cn

Authors

Huifen Hu − *Henan Key Laboratory of Polyoxometalate Chemistry, College of Chemistry and Chemical Engineering, Henan University, Kaifeng, Henan 475004, China*

Jingjing Pang − *Henan Key Laboratory of Polyoxometalate Chemistry, College of Chemistry and Chemical Engineering, Henan University, Kaifeng, Henan 475004, China*

Peijun Gong − *Henan Key Laboratory of Polyoxometalate Chemistry, College of Chemistry and Chemical Engineering, Henan University, Kaifeng, Henan 475004, China*

Complete contact information is available at: https://pubs.acs.org/10.1021/acs.inorgchem.0c00768

Notes

The authors declare no competing financial interest.

ACKNOWLEDGMENTS

Our research has been funded by the NNSF of China (Grants 21771052, 21671054, 21871077, and 21571048), the Program for Innovation Teams in Science and Technology in Universities of Henan Province (Grant 20IRTSTHN004), and the First-Class Discipline Cultivation Project of Henan University (Grants 2019YLZDYJ02 and CJ1205A0240019).

REFERENCES

(1) Yin, Q.; Tan, J. M.; Besson, C.; Geletii, Y. V.; Musaev, D. G.; Kuznetsov, A. E.; Luo, Z.; Hardcastle, K. I.; Hill, C. L. A fast soluble carbon-free molecular water oxidation catalyst based on abundant metals. *Science* **2010**, *328*, 342−345.

(2) Zhao, J.-W.; Li, Y.-Z.; Chen, L.-J.; Yang, G.-Y. Research progress on polyoxometalate-based transition-metal−rare-earth heterometallic derived materials: synthetic strategies, structural overview and functional applications. *Chem. Commun.* **2016**, *52*, 4418−4445.

(3) Clemente-Juan, J. M.; Coronado, E.; Gaita-Ariño, A. Magnetic polyoxometalates: from molecular magnetism to molecular spintronics and quantum computing. *Chem. Soc. Rev.* **2012**, *41*, 7464−7478.

(4) Kumar, D.; Derat, E.; Khenkin, A. M.; Neumann, R.; Shaik, S. The high-valent iron-oxo species of polyoxometalate, if it can be made, will be a highly potent catalyst for CH hydroxylation and double-bond epoxidation. *J. Am. Chem. Soc.* **2005**, *127*, 17712−17718.
(5) Ma, P.; Hu, F.; Wang, J.; Niu, J. Carboxylate covalently modified polyoxometalates: from synthesis, structural diversity to applications. *Coord. Chem. Rev.* **2019**, *378*, 281−309.
(6) Liu, J.-C.; Han, Q.; Chen, L.-J.; Zhao, J.-W.; Streb, C.; Song, Y.-F. Aggregation of giant cerium-bismuth tungstate clusters into a 3D porous framework with high proton conductivity. *Angew. Chem., Int. Ed.* **2018**, *57*, 8416−8420.
(7) Keana, J. F. W.; Ogan, M. D.; Lu, Y. X.; Beer, M.; Varkey, J. Functionalized Keggin- and Dawson-type cyclopentadienyltitanium heteropolytungstate anions: small, individually distinguishable labels for conventional transmission electron microscopy. 2. Reactions. *J. Am. Chem. Soc.* **1986**, *108*, 7957−7963.
(8) Rapko, B. M.; Pohl, M.; Finke, R. G. Synthesis, isolation, and spectroscopic characterization of trivanadium polyoxoanion-supported $(C_5H_5)Ti^{3+}$: $(Bu_4N)_4[CpTi{\cdot}SiW_9V_3O_{40}]$ and $(Bu_4N)_6[CpTi{\cdot}P_2W_{15}V_3O_{62}]$. *Inorg. Chem.* **1994**, *33*, 3625−3634.
(9) Laurencin, D.; Villanneau, R.; Herson, P.; Thouvenot, R.; Jeannin, Y.; Proust, A. A new organometallic heteropolytungstate related to $[Sb_2W_{22}O_{74}(OH)_2]^{12-}$: synthesis and structural characterisation of the bis-$\{Ru(p\text{-cymene})\}^{2+}$-containing anion $[Sb_2W_{20}O_{70}\{Ru(p\text{-cymene})\}_2]^{10-}$. *Chem. Commun.* **2005**, *44*, 5524−5526.
(10) Mal, S. S.; Nsouli, N. H.; Dickman, M. H.; Kortz, U. Organoruthenium derivative of the cyclic $[H_7P_8W_{48}O_{184}]^{33-}$ anion: $[\{K(H_2O)\}_3\{Ru(p\text{-cymene})(H_2O)\}_4P_8W_{49}O_{186}(H_2O)_2]^{27-}$. *Dalton Trans.* **2007**, *25*, 2627−2630.
(11) Wei, X. Y.; Dickman, M. H.; Pope, M. T. Rhodium−carbon bond formation in aqueous solution. Synthesis, structure, and reactivity of the functionalized heteropolytungstates, $[XW_{11}O_{39}RhCH_2COOH]^{5,6-}$ (X = P, Si). *J. Am. Chem. Soc.* **1998**, *120*, 10254−10255.
(12) Li, J. X.; Zhai, F. Y.; Wang, X. H.; Li, E. M.; Zhang, S. D.; Zhang, Q. L.; Du, X. G. Synthesis and biological activity of triorganogermanium substituted heteropolytungstates. *Polyhedron* **2008**, *27*, 1150−1154.
(13) Knoth, W. H. Derivatives of heteropolyanions. 1. organic derivatives of $W_{12}SiO_{40}^{4-}$, $W_{12}PO_{40}^{3-}$, and $Mo_{12}SiO_{40}^{4-}$. *J. Am. Chem. Soc.* **1979**, *101*, 759−760.
(14) Wang, X. H.; Dai, H. C.; Liu, J. F. Synthesis and characterization of organotin-substituted heteropoly tungstosilicates and their biological activity I. *Polyhedron* **1999**, *18*, 2293−2300.
(15) Sazani, G.; Dickman, M. H.; Pope, M. T. Organotin derivatives of α-$[X^{III}W_9O_{33}]^{9-}$ (X = As, Sb) heteropolytungstates. Solution- and solid-state characterization of $[\{(C_6H_5Sn)_2O\}_2H(\alpha\text{-}AsW_9O_{33})_2]^{9-}$ and $[(C_6H_5Sn)_3\ Na_3(\alpha\text{-}SbW_9O_{33})_2]^{6-}$. *Inorg. Chem.* **2000**, *39*, 939−943.
(16) Bareyt, S.; Piligkos, S.; Hasenknopf, B.; Gouzerh, P.; Lacôte, E.; Thorimbert, S.; Malacria, M. Highly efficient peptide bond formation to functionalized Wells-Dawson-type polyoxotungstates. *Angew. Chem., Int. Ed.* **2003**, *42*, 3404−3406.
(17) Hussain, F.; Kortz, U.; Clark, R. J. The bis-phenyltin-substituted, lone-pair-containing tungstoarsenate $[(C_6H_5Sn)_2As_2W_{19}O_{67}(H_2O)]^{8-}$. *Inorg. Chem.* **2004**, *43*, 3237−3241.
(18) Hussain, F.; Kortz, U. Polyoxoanions functionalized by diorganotin groups: the tetrameric, chiral tungstoarsenate(III), $[\{Sn(CH_3)_2(H_2O)\}_2\{Sn(CH_3)_2\}As_3(\alpha\text{-}AsW_9O_{33})_4]^{21-}$. *Chem. Commun.* **2005**, *9*, 1191−1193.
(19) Micoine, K.; Hasenknopf, B.; Thorimbert, S.; Lacôte, E.; Malacria, M. A general strategy for ligation of organic and biological molecules to Dawson and Keggin polyoxotungstates. *Org. Lett.* **2007**, *9*, 3981−3984.
(20) Bar-Nahum, I.; Ettedgui, J.; Konstantinovski, L.; Kogan, V.; Neumann, R. A new method for the synthesis of organopolyoxometalate hybrid compounds. *Inorg. Chem.* **2007**, *46*, 5798−5804.
(21) Boglio, C.; Micoine, K.; Derat, E.; Thouvenot, R.; Hasenknopf, B.; Thorimbert, S.; Lacôte, E.; Malacria, M. Regioselective activation of oxo ligands in functionalized Dawson polyoxotungstates. *J. Am. Chem. Soc.* **2008**, *130*, 4553−4561.
(22) Piedra-Garza, L. F.; Dickman, M. H.; Moldovan, O.; Breunig, H. J.; Kortz, U. Organoantimony-containing polyoxometalate: $[\{PhSbOH\}_3(A\text{-}\alpha\text{-}PW_9O_{34})_2]^{9-}$. *Inorg. Chem.* **2009**, *48*, 411−413.
(23) Xin, F. B.; Pope, M. T.; Long, G. J.; Russo, U. Polyoxometalate derivatives with multiple organic groups. 2. Synthesis and structures of tris(organotin) α, β-Keggin tungstosilicates. *Inorg. Chem.* **1996**, *35*, 1207−1213.
(24) Reinoso, S.; Bassil, B. S.; Barsukova, M.; Kortz, U. pH-controlled assemblies of dimethyltin-functionalized 9-tungstophosphates with guanidinium as structure-directing cation. *Eur. J. Inorg. Chem.* **2010**, *2010*, 2537−2542.
(25) Bareyt, S.; Piligkos, S.; Hasenknopf, B.; Gouzerh, P.; Lacôte, E.; Thorimbert, S.; Malacria, M. Efficient preparation of functionalized hybrid organic/inorganic Wells-Dawson-type polyoxotungstates. *J. Am. Chem. Soc.* **2005**, *127*, 6788−6794.
(26) Hussain, F.; Reicke, M.; Kortz, U. The hybrid organic-inorganic 2-D material $(CsNa_2[\{Sn(CH_3)_2\}_3(H_2O)_4(\beta\text{-}XW_9O_{33})]{\cdot}7H_2O)_\infty$ (X = As^{III}, Sb^{III}) and its solution properties. *Eur. J. Inorg. Chem.* **2004**, *2004*, 2733−2738.
(27) Hussain, F.; Kortz, U.; Keita, B.; Nadjo, L.; Pope, M. T. Tetrakis(dimethyltin)-containing tungstophosphate $[\{Sn(CH_3)_2\}_4(H_2P_4\ W_{24}O_{92})_2]^{28-}$: first evidence for a lacunary preyssler ion. *Inorg. Chem.* **2006**, *45*, 761−766.
(28) Kortz, U.; Hussain, F.; Reicke, M. The ball-shaped heteropolytungstates $[\{Sn(CH_3)_2(H_2O)\}_{24}\{Sn(CH_3)_2\}_{12}(A\text{-}XW_9O_{34})_{12}]^{36-}$. *Angew. Chem., Int. Ed.* **2005**, *44*, 3773−3777.
(29) Piedra-Garza, L. F.; Reinoso, S.; Dickman, M. H.; Sanguineti, M. M.; Kortz, U. The first 3-dimensional assemblies of organotin-functionalized polyanions. *Dalton Trans.* **2009**, *0*, 6231−6234.
(30) Zhang, L. C.; Zheng, S. L.; Xue, H.; Zhu, Z. M.; You, W. S.; Li, Y. G.; Wang, E. B. New tetra(organotin)-decorated boat-like polyoxometalate. *Dalton Trans.* **2010**, *39*, 3369−3371.
(31) Zhang, L. C.; Xue, H.; Zhu, Z. M.; Wang, Q.-X.; You, W. S.; Li, Y. G.; Wang, E.-B. New estertin derivatives based on trivacant Keggin-type $[\beta\text{-}SbW_9O_{33}]^{9-}$ cluster. *Inorg. Chem. Commun.* **2010**, *13*, 609−612.
(32) Wang, Z. J.; Zhang, L. C.; Zhu, Z. M.; Chen, W. L.; You, W. S.; Wang, E. B. Two new sandwich-type tungstobismuthates constructed from trivacant Keggin units, estertin and transition metals. *Inorg. Chem. Commun.* **2012**, *17*, 151−154.
(33) Sang, X. J.; Li, J. S.; Zhang, L. C.; Wang, Z. J.; Chen, W. L.; Zhu, Z. M.; Su, Z. M.; Wang, E. B. A novel carboxyethyltin functionalized sandwich-type germanotungstate: synthesis, crystal structure, photosensitivity, and application in dye-sensitized solar cells. *ACS Appl. Mater. Interfaces* **2014**, *6*, 7876−7884.
(34) Bai, J. P.; Su, F.; Zhu, H. T.; Sun, H.; Zhang, L. C.; Liu, M. Y.; You, W. S.; Zhu, Z. M. An open chain carboxyethyltin functionalized sandwich-type tungstophosphate based on a trivacant Dawson subunit: synthesis, characterization and properties. *Dalton Trans.* **2015**, *44*, 6423−6430.
(35) Zhang, B.; Zhang, L. C.; Zhang, Y. J.; Su, F.; You, W. S.; Zhu, Z. M. Two Keggin sandwich-type tungstophosphates modified by open-chain carboxyethyltin groups and transition metals. *RSC Adv.* **2015**, *5*, 47319−47325.
(36) Wu, C. D.; Lu, C. Z.; Zhuang, H. H.; Huang, J. S. Hydrothermal assembly of a novel three-dimensional framework formed by $[GdMo_{12}O_{42}]^{9-}$ anions and nine coordinated Gd^{III} cations. *J. Am. Chem. Soc.* **2002**, *124*, 3836−3837.
(37) Chen, W. L.; Li, Y. G.; Wang, Y. H.; Wang, E. B.; Zhang, Z. M. A new polyoxometalate-based 3d−4f heterometallic aggregate: a model for the design and synthesis of new heterometallic clusters. *Dalton Trans.* **2008**, *7*, 865−867.
(38) Li, H. L.; Liu, Y. J.; Zheng, R.; Chen, L. J.; Zhao, J. W.; Yang, G. Y. Trigonal pyramidal $\{AsO_2(OH)\}$ bridging tetranuclear rare-earth

https://dx.doi.org/10.1021/acs.inorgchem.0c00768
Inorg. Chem. 2020, 59, 11287−11297

encapsulated polyoxotungstate aggregates. *Inorg. Chem.* **2016**, *55*, 3881−3893.
(39) Ritchie, C.; Moore, E. G.; Speldrich, M.; Kögerler, P.; Boskovic, C. Terbium polyoxometalate organic complexes: correlation of structure with luminescence properties. *Angew. Chem., Int. Ed.* **2010**, *49*, 7702−7705.
(40) Wang, S. S.; Yang, G. Y. Recent advances in polyoxometalate-catalyzed reactions. *Chem. Rev.* **2015**, *115*, 4893−4962.
(41) Boglio, C.; Lemière, G.; Hasenknopf, B.; Thorimbert, S.; Lacôte, E.; Malacria, M. Lanthanide complexes of the monovacant Dawson polyoxotungstate $[\alpha_1\text{-}P_2W_{17}O_{61}]^{10-}$ as selective and recoverable lewis acid catalysts. *Angew. Chem., Int. Ed.* **2006**, *45*, 3324−3327.
(42) Liu, J. C.; Han, Q.; Chen, L. J.; Zhao, J. W.; Streb, C.; Song, Y. F. Aggregation of giant cerium−bismuth tungstate clusters into a 3D porous framework with high proton conductivity. *Angew. Chem.* **2018**, *130*, 8552−8556.
(43) Li, Z.; Li, X. X.; Yang, T.; Cai, Z. W.; Zheng, S. T. Four-shell polyoxometalates featuring high-nuclearity Ln_{26} clusters: structural transformations of nanoclusters into frameworks triggered by transition-metal ions. *Angew. Chem., Int. Ed.* **2017**, *56*, 2664−2669.
(44) Han, Q.; Liu, J. C.; Wen, Y.; Chen, L. J.; Zhao, J. W.; Yang, G. Y. Tellurotungstate-based organotin−rare-earth heterometallic hybrids with four organic components. *Inorg. Chem.* **2017**, *56*, 7257−7269.
(45) Liu, J. L.; Jin, M. T.; Chen, L. J.; Zhao, J. W. First dimethyltin-functionalized rare-earth incorporated tellurotungstates consisting of $\{B\text{-}\alpha\text{-}TeW_7O_{28}\}$ and $\{W_5O_{18}\}$ mixed building units. *Inorg. Chem.* **2018**, *57*, 12509−12520.
(46) Brown, I. D.; Altermatt, D. Bond-valence parameters obtained from a systematic analysis of the inorganic crystal structure database. *Acta Crystallogr., Sect. B: Struct. Sci.* **1985**, *B41*, 244−247.
(47) Kortz, U.; Savelieff, M. G.; Bassil, B. S.; Keita, B.; Nadjo, L. Synthesis and characterization of iron(III)-substituted, dimeric polyoxotungstates, $[Fe_4(H_2O)_{10}(\beta\text{-}XW_9O_{33})_2]^{n-}$ (n = 6, X = As^{III}, Sb^{III}; n = 4, X = Se^{IV}, Te^{IV}). *Inorg. Chem.* **2002**, *41*, 783−789.
(48) Ismail, A. H.; Bassil, B. S.; Römer, I.; Kortz, U. Z. Mono- and di-lanthanide derivatives of 22-tungsto-2-antimonate(III), $[Ln(H_2O)_4Sb_2W_{21}O_{72}(OH)]^{10-}$ and $[Ln_2(H_2O)_8Sb_2W_{20}O_{70})]^{8-}$. *Z. Anorg. Allg. Chem.* **2013**, *639*, 2510−2515.
(49) Jia, J. G.; Zhang, Y. H.; Zhang, P. P.; Ma, P. T.; Zhang, D. D.; Wang, J. P.; Niu, J. Y. Synthesis and characterization of a series of novel polyoxometalate-supported carbonyl manganese derivatives. *RSC Adv.* **2016**, *6*, 108335−108342.
(50) Bünzli, J. C. G.; Piguet, C. Taking advantage of luminescent lanthanide ions. *Chem. Soc. Rev.* **2005**, *34*, 1048−1077.
(51) Armelao, L.; Quici, S.; Barigelletti, F.; Accorsi, G.; Bottaro, G.; Cavazzini, M.; Tondello, E. Design of luminescent lanthanide complexes: from molecules to highly efficient photo-emitting materials. *Coord. Chem. Rev.* **2010**, *254*, 487−505.
(52) Rocha, J.; Carlos, L. D.; Paz, F. A. A.; Ananias, D. Luminescent multifunctional lanthanides-based metal-organic frameworks. *Chem. Soc. Rev.* **2011**, *40*, 926−940.
(53) Liu, Y.; Tu, D.; Zhu, H.; Chen, X. Lanthanide-doped luminescent nanoprobes: controlled synthesis, optical spectroscopy, and bioapplications. *Chem. Soc. Rev.* **2013**, *42*, 6924−6958.
(54) Sopasis, G. J.; Orfanoudaki, M.; Zarmpas, P.; Philippidis, A.; Siczek, M.; Lis, T.; O'Brien, J. R.; Milios, C. J. 2-aminoisobutyric acid in Co(II) and Co(II)/Ln(III) chemistry: homometallic and heterometallic clusters. *Inorg. Chem.* **2012**, *51*, 1170−1179.
(55) Kuriki, K.; Koike, Y.; Okamoto, Y. Plastic optical fiber lasers and amplifiers containing lanthanide complexes. *Chem. Rev.* **2002**, *102*, 2347−2356.
(56) Koester, C. J.; Snitzer, E. Amplification in a fiber laser. *Appl. Opt.* **1964**, *3*, 1182−1186.
(57) Yajima, H.; Kawase, S.; Sekimoto, Y. Amplification at 1.06 μm using a Nd: glass thin−film waveguide. *Appl. Phys. Lett.* **1972**, *21*, 407−409.
(58) Soares-Santos, P. C. R.; Cunha-Silva, L.; Paz, F. A. A.; Ferreira, R. A. S.; Rocha, J.; Carlos, L. D.; Nogueira, H. I. S. Photoluminescent lanthanide- organic bilayer networks with 2,3-pyrazinedicarboxylate and oxalate. *Inorg. Chem.* **2010**, *49*, 3428−3440.
(59) Cui, Y. J.; Yue, Y. F.; Qian, G. D.; Chen, B. L. Luminescent functional metal−organic frameworks. *Chem. Rev.* **2012**, *112*, 1126−1162.
(60) Wang, X. F.; Liu, C. S.; Yu, T. H.; Yan, X. H. Controlled synthesis, photoluminescence, and the quantum cutting mechanism of Eu^{3+} doped $NaYbF_4$ nanotubes. *Phys. Chem. Chem. Phys.* **2014**, *16*, 13440−13446.
(61) Kirby, A. F.; Richardson, F. S. Detailed analysis of the optical absorption and emission spectra of Eu^{3+} in the trigonal (C3) $Eu(DBM)_3{\cdot}H_2O$ system. *J. Phys. Chem.* **1983**, *87*, 2544−2556.
(62) Su, Y.; Li, L.; Li, G. Synthesis and optimum luminescence of $CaWO_4$-based red phosphors with codoping of Eu^{3+} and Na^+. *Chem. Mater.* **2008**, *20*, 6060−6067.
(63) Mialane, P.; Lisnard, L.; Mallard, A.; Marrot, J.; Antic-Fidancev, E.; Aschehoug, P.; Vivien, D.; Secheresse, F. Solid-state and solution´ studies of $\{Ln_n(SiW_{11}O_{39})\}$ polyoxoanions: an example of building block condensation dependent on the nature of the rare earth. *Inorg. Chem.* **2003**, *42*, 2102−2108.
(64) Beeby, A.; Clarkson, I. M.; Dickins, R. S.; Faulkner, S.; Parker, D.; Royle, L.; de Sousa, A. S.; Williams, J. A. G.; Woods, M. Non-radiative deactivation of the excited states of europium, terbium and ytterbium complexes by proximate energy-matched OH, NH and CH oscillators:an improved luminescence method for establishing solution hydration states. *J. Chem. Soc., Perkin Trans. 2* **1999**, 493−504.
(65) Tan, J.; He, S.; Yan, S.; Li, Y.; Li, H.; Zhang, H.; Zhao, L.; Li, L. Exogenous EDDS modifies copper-induced various toxic responses in rice. *Protoplasma* **2014**, *251*, 1213−1221.
(66) Zhang, X.; Zhao, X.; Li, B.; Xia, J.; Miao, Y. SRO1 regulates heavy metal mercury stress response in Arabidopsis thaliana. *Chin. Sci. Bull.* **2014**, *59*, 3134−3141.
(67) Zhao, B.; Chen, X.-Y.; Cheng, P.; Liao, D.-Z.; Yan, S.-P.; Jiang, Z.-H. Coordination polymers containing 1D channels as selective luminescent probes. *J. Am. Chem. Soc.* **2004**, *126*, 15394−15395.
(68) Evans, J. D.; Sumby, C. J.; Doonan, C. J. Post-synthetic metalation of metal−organic frameworks. *Chem. Soc. Rev.* **2014**, *43*, 5933−5951.
(69) Huang, W. H.; Ren, J.; Yang, Y. H.; Li, X. M.; Wang, Q.; Jiang, N.; Yu, J. Q.; Wang, F.; Zhang, J. Water-stable metal−organic frameworks with selective sensing on Fe^{3+} and nitroaromatic explosives, and stimuli-responsive luminescence on lanthanide encapsulation. *Inorg. Chem.* **2019**, *58*, 1481−1491.
(70) Yang, Y. J.; Wang, M. J.; Zhang, K. L. A novel photo-luminescent Cd(II)−organic framework exhibiting rapid and efficient multi-responsive fluorescence sensing for trace amounts of Fe^{3+} ions and some NACs, especially for 4-nitroaniline and 2-methyl-4-nitroaniline. *J. Mater. Chem. C* **2016**, *4*, 11404−11418.
(71) Xiao, Y. Q.; Cui, Y. J.; Zheng, Q.; Xiang, S. C.; Qian, G. D.; Chen, B. L. A microporous luminescent metal−organic framework for highly selective and sensitive sensing of Cu^{2+} in aqueous solution. *Chem. Commun.* **2010**, *46*, 5503−5505.
(72) Chen, B. L.; Wang, L. B.; Xiao, Y. Q.; Fronczek, F. R.; Xue, M.; Cui, Y. J.; Qian, G. D. A luminescent metal−organic framework with Lewis basic pyridyl sites for the sensing of metal ions. *Angew. Chem.* **2009**, *121*, 508−511.
(73) Li, Z. J.; Li, X. Y.; Yan, Y. T.; Hou, L.; Zhang, W. Y.; Wang, Y. Y. Tunable emission and selective luminescence sensing in a series of lanthanide metal−organic frameworks with uncoordinated Lewis basic triazolyl sites. *Cryst. Growth Des.* **2018**, *18*, 2031−2039.
(74) Xu, X. Y.; Yan, B. Eu(III) functionalized Zr-based metal-organic framework as excellent fluorescent probe for Cd^{2+} detection in aqueous environment. *Sens. Actuators, B* **2016**, *222*, 347−353.
(75) Zhao, J.; Wang, Y. N.; Dong, W. W.; Wu, Y. P.; Li, D.-S.; Zhang, Q. C. A robust luminescent Tb(III)-MOF with Lewis basic

https://dx.doi.org/10.1021/acs.inorgchem.0c00768
Inorg. Chem. 2020, 59, 11287−11297

pyridyl sites for the highly sensitive detection of metal ions and small molecules. *Inorg. Chem.* **2016**, *55*, 3265−3271.
(76) Zhou, J. M.; Shi, W.; Li, H. M.; Li, H.; Cheng, P. Experimental studies and mechanism analysis of high-sensitivity luminescent sensing of pollutional small molecules and ions in Ln_4O_4 cluster based microporous metal−organic frameworks. *J. Phys. Chem. C* **2014**, *118*, 416−426.
(77) Liu, B.; Wu, W. P.; Hou, L.; Wang, Y. Y. Four uncommon nanocage-based Ln-MOFs: highly selective luminescent sensing for Cu^{2+} ions and selective CO_2 capture. *Chem. Commun.* **2014**, *50*, 8731−8734.
(78) Liu, C.; Yan, B. Zeolite-type metal organic frameworks immobilized Eu^{3+} for cation sensing in aqueous environment. *J. Colloid Interface Sci.* **2015**, *459*, 206−211.
(79) Zhao, B.; Chen, X. Y.; Cheng, P.; Liao, D. Z.; Yan, S. P.; Jiang, Z. H. Coordination polymers containing 1D channels as selective luminescent probes. *J. Am. Chem. Soc.* **2004**, *126*, 15394−15395.
(80) Wang, P.; Wu, J. Highly selective and sensitive detection of Zn (II) and Cu (II) ions using a novel peptide fluorescent probe by two different mechanisms and its application in live cell imaging. *Spectrochim. Acta, Part A* **2019**, *208*, 140−149.
(81) Pang, B.-J.; Li, C.-R.; Yang, Z.-Y. A novel chromone and rhodamine derivative as fluorescent probe for the detection of Zn(II) and Al(III) based on two different mechanisms. *Spectrochim. Acta, Part A* **2018**, *204*, 641−647.
(82) Shyamal, M.; Mazumdar, P.; Maity, S.; Samanta, S.; Sahoo, G. P.; Misra, A. Misra, Highly selective turn-on fluorogenic chemosensor for robust quantification of Zn(II) based on aggregation induced emission enhancement feature. *ACS Sens.* **2016**, *1*, 739−747.
(83) Xue, J.; Tian, L.-M.; Yang, Z.-Y. A novel rhodamine-chromone Schiff-base as turn-on fluorescent probe for the detection of Zn (II) and Fe (III) in different solutions. *J. Photochem. Photobiol., A* **2019**, *369*, 77−84.
(84) Zhao, G.; Guo, B.-Y.; Wei, G.; Guang, S.-Y.; Gu, Z.-Y.; Xu, H.-Y. A novel dual-channel Schiff base fluorescent chemo-sensor for Zn^{2+} and Ca^{2+} recognition: Synthesis, mechanism and application. *Dyes Pigm.* **2019**, *170*, 107614.

https://dx.doi.org/10.1021/acs.inorgchem.0c00768
Inorg. Chem. 2020, 59, 11287−11297